Stability analysis of Rayleigh-Bénard convection in a cylinder with internal heat generation

Bo-Fu Wang
Shanghai Institute of Applied Mathematics and Mechanics, and Shanghai Key Laboratory of Mechanics in Energy Engineering, Shanghai University, Shanghai 200072, China

Lin Zhou
Institute of Structural Mechanics, Chinese Academy of Engineering Physics, Mianyang, 621900, China

Zhen-Hua Wan*
Department of Modern Mechanics, University of Science and Technology of China, Hefei 230027, China

Dong-Jun Ma
Institute of Applied Physics and Computational Mathematics, Beijing 100088, China

De-Jun Sun
Department of Modern Mechanics, University of Science and Technology of China, Hefei 230027, China
(Received 21 April 2016; published 14 July 2016)

The flow instabilities of Rayleigh-Bénard convection in a cylinder with effect of uniform internal heat source are investigated numerically. The instabilities of the static state and of axisymmetric flows are investigated by linear stability analysis. The convection threshold depends on the strength of internal heat source q and the aspect ratio of the cylinder Γ. The stability of axisymmetric flows is strongly affected by these two parameters, as well as the Prandtl number Pr. Depending on the value of q, three regimes are identified: weak internal heating, moderate internal heating, and strong internal heating regime. In a weak internal heating regime, the instability characteristics are similar to Rayleigh-Bénard convection. In a moderate internal heating regime, intense interaction of buoyancy instability and hydrodynamic instability result in complex instability curves. When q is large enough, the internal heating effect overwhelms the boundary heating effect. Specifically, the influence of Pr on instability is studied at a moderate internal heat strength $q = 6.4$. An extremely multivalued stability curve is observed. At most five critical Rayleigh numbers can be determined for the axisymmetry-breaking instability at a certain Prandtl number. An axisymmetric unsteady instability mode is observed as well. By nonlinear simulation, the oscillatory flow patterns are obtained, and the axisymmetry-breaking bifurcation of the unsteady toroidal flow is studied.

DOI: 10.1103/PhysRevE.94.013108

I. INTRODUCTION

Convection induced by internal heat generation usually occurs in geophysical, astrophysical, and industrial processes. For example, heat produced by radioactive decay of elements [1] can drive convection in earth's mantle, absorption of heat from sunlight yields motion in the atmosphere [2], and a nuclear fusion reaction causes volumetric heat production in stellar interiors and the resulting convection is crucial for studying the history of stars and other astronomical events [3], and internal heating also arises from chemical reactions and electric heating [4]. The studies of internal heated convection generally uses idealized models of thermal convection in horizontal fluid layers, such as a fluid layer bounded below by a perfect insulator and above by a perfect conductor, a fluid layer bounded by two perfect conductors with equal temperature, and a fluid layer bounded by two perfect conductors with higher temperature below and lower temperature above [5]. The first configuration is most commonly studied; however, the other two have received relatively less attention.

Unlike Rayleigh-Bénard convection in a fluid layer, which has been intensively studied by theoretical, experimental, and numerical approaches, convection driven by internal heating is mostly investigated theoretically and numerically due to the difficulties in laboratory experiments. For the configuration with insulated lower boundary and fixed top boundary temperature, the first experiment has been conducted by Tritton and Zarraga [6] using Joule heating in a fluid layer. They found that the development of cellular patterns with varied Rayleigh number in many respects is similar to the observations in Rayleigh-Bénard convections. However, two major differences were found as well. The first difference is that the cell structure is formed by fluid descending in the center and ascending in the periphery, and the other is the large increases in cell scales in the horizontal direction with an increase in Rayleigh number. Theoretical studies [7–9] seem unable to fully explain the observed phenomena. The elongation of cell patterns had once been regarded as the result of nonuniformity of internal heat generation in the experimental apparatus rather than an intrinsic feature of this problem. Until recently, a series of experimental and numerical studies confirmed this phenomenon to be an intrinsic feature of internally heated convection [10–12].

When the fluid layer is confined between two perfect conductors with either equal temperature or higher temperature from below, the flow becomes complicated due to the presence

*wanzh@ustc.edu.cn.

of a stably stratified layer near the bottom. Several experiments were primarily conducted in the 1970s to study the convection in a fluid layer heated internally by electric currents [13,14], where the top and bottom temperatures were kept as close to equal as possible. Tveitereid [15] theoretically predicted the hexagons patterns and a subcritical region. Experiments using periodically distributed heaters in air were performed more recently [16]. Numerical simulations have been performed for two-dimensional [14,17] and three-dimensional [18] systems. The space- and time-averaged temperature of an infinite Prandtl number fluid confined between isothermal no-slip boundaries driven by uniform internal heating was derived theoretically [19]. Deshmukh *et al.* [20] mainly considered natural convection in two-dimensional horizontal and inclined square enclosures with uniform heat generation, and they performed a parametric study to evaluate different influence factors on flow pattern. Furthermore, they conducted three-dimensional simulations and found that the critical Rayleigh number for transition from steady to oscillation is higher than that of the two-dimensional cases. Very recently, Goluskin and Spiegel [21,22] conducted direct numerical simulations of two- and three-dimensional internally heated convection for wide ranges of Prandtl number and Rayleigh number, and they discussed the scaling of mean temperature and heat-flux asymmetry. Some numerical simulations and experiments relevant to accidents in nuclear reactor engineering were performed as well [23–25], where the configurations considered were related to particular applications.

The present study is concerned with instability of Rayleigh-Bénard convection in a cylinder with internal heat generation. Convection simultaneously driven by boundary and internal heating exists widely in nature and engineering applications. Nonetheless, this issue is rarely mentioned in the previous literature. Perekattu and Balaji [26] performed linear stability analysis for both finite and infinite two-dimensional cavities, and the effect of aspect ratio on the onset of convection is evaluated. Kolmychkov *et al.* [27] numerically studied linear instability and flow patterns. They investigated the flow structure for Prandtl number ranging from 0.1 to 100 and considered both subcritical and supercritical flow patterns. In this study, the onset of convection and stability of axisymmetric flow (secondary instability) of the dually driven convection in a cylinder are analyzed. The results are compared with that of solely boundary driven convection. The oscillatory flow patterns beyond instability are simulated, and their evolution with control parameter is presented.

II. MATHEMATICAL FORMULATION AND NUMERICAL METHOD

We studied Rayleigh-Bénard convection with internal heat source in a cylinder of depth H and radius R. The aspect ratio is defined by $\Gamma = R/H$. The problem is considered in cylindrical coordinates (r,φ,z), where r denotes radial coordinate, φ denotes azimuthal coordinate, and z denotes vertical coordinate. The fluid has kinematic viscosity ν, density ρ, thermal diffusivity κ, and thermal expansion coefficient α. The top and bottom of the cylinder are assumed to be perfectly conducting and kept at constant temperatures T_c and T_h ($T_h > T_c$), respectively. The lateral wall is adiabatic. We use the units H, H^2/ν, ν/H, and $\rho(\nu/H)^2$ for length, time, velocity, and pressure, respectively. The dimensionless temperature is defined by $\Theta = (T - T_c)/(T_h - T_c)$. The governing equations in dimensionless form are

$$\nabla \cdot u = 0, \tag{1}$$

$$\frac{\partial u}{\partial t} + u \cdot \nabla u = -\nabla p + \nabla^2 u + \frac{\mathrm{Ra}}{\mathrm{Pr}} \Theta \, \mathbf{e}_z, \tag{2}$$

$$\frac{\partial \Theta}{\partial t} + u \cdot \nabla \Theta = \frac{1}{\mathrm{Pr}} \nabla^2 \Theta + \frac{1}{\mathrm{Pr}} q, \tag{3}$$

where p is the pressure and u is the three-dimensional velocity field $u = (u_r, u_\varphi, u_z)$. The Prandtl number is $\mathrm{Pr} = \nu/\kappa$, the Rayleigh number is $\mathrm{Ra} = g\alpha(T_h - T_c)H^3/(\nu\kappa)$, q is the heat source, and $\mathbf{e}_z$ is a unit vector in the vertical direction. The basic state of pure conduction is described by the velocity $u = \mathbf{0}$ and the temperature distribution $\Theta(z) = 1 - z + z(1-z)q/2$. The conduction state solution is taken as the initial condition in our nonlinear simulation. The boundary conditions are all assumed to be no-slip, the top and bottom walls are conducting, and the side wall is insulating:

$$u_r = u_\varphi = u_z = 0, \quad \Theta = 1 \quad \text{at} \quad z = 0, \tag{4}$$

$$u_r = u_\varphi = u_z = 0, \quad \Theta = 0 \quad \text{at} \quad z = 1, \tag{5}$$

$$u_r = u_\varphi = u_z = 0, \quad \frac{\partial \Theta}{\partial r} = 0 \quad \text{at} \quad r = \Gamma. \tag{6}$$

The governing equations are discretized on a structured grid in cylindrical coordinates. A uniform mesh is employed in the azimuthal direction, while a nonuniform mesh is used in the radial and axial directions, with mesh points concentrated toward the boundaries. The time-dependent solutions of the governing equations are obtained by using a second-order fractional step method in three-dimensional cylindrical coordinates [28]. The viscous terms are discretized in time using an implicit Crank-Nicolson scheme, whereas an explicit Adams-Bashforth scheme is employed for the nonlinear terms [29]. A second-order-accuracy central difference method on a staggered grid is used for spatial discretization.

In this study we consider the instability for both onset of convection and axisymmetric flow. The base flow for the stability analysis of convection threshold is analytical, i.e., the conduction solution. The nonstatic axisymmetric base flow is captured by a Jacobian-free Newton-Krylov method, which is able to calculate the stable and unstable steady-state solutions [30]. The leading eigenvalues and corresponding eigenvectors of the control equations linearized about the base flow are determined using the Arnoldi algorithm from the ARPACK library [31]. The linearized control equations can be written as $\partial_t q' = (\mathbf{N}_u + \mathbf{L})q'$, where $q' = (u', \Theta')$ are perturbations, and $\mathbf{N}_u$ and $\mathbf{L}$ are linearized convection and diffusion operator, respectively. When considering $q' = \hat{q}e^{\mu t}$, we have the eigenvalue problem $(\mathbf{N}_u + \mathbf{L})\hat{q} = \mu\hat{q}$. This eigenvalue problem is not directly solved to avoid large computational cost. Using an alternative approach by time-stepping the linearized equations [30], we are able to construct a small matrix which represents the action of the Jacobian $(\mathbf{N}_u + \mathbf{L})$ on the subspace of leading eigenvectors. The eigensolution of this matrix gives the leading eigenvalues and eigenvectors.

III. RESULTS

A. Onset of convection

Similar to Rayleigh-Bénard convection, the primary state at a low Rayleigh number is static. The temperature profile is shown in Fig. 1. It can be observed that the distribution of temperature is close to that of Rayleigh-Bénard convection with weak internal heat strength, and the internal heating becomes predominant at large values of q. The internal heating and heating from below both play essential roles at a moderate value of q (around 6). The stability curves for the onset of convection at different aspect ratios $\Gamma = 0.5, 1, 2, 4$ are shown in Fig. 2. This instability for convection threshold is independent on the Prandtl number, which is the same as Rayleigh-Bénard convection. The critical Rayleigh number (Ra_{cr}) decreases with the increase of Γ at small values of q, which also decreases with increasing q for each aspect ratio Γ. Given the fact that convection can be driven by pure internal heating without bottom heating, Ra_{cr} will approach zero at a finite q. The decrease rate of Ra_{cr} is rapid for $\Gamma = 0.5$ and slow for $\Gamma = 1, 2, 4$. The critical Rayleigh number for $\Gamma = 0.5$ becomes smaller than the other three when q is greater than 7.3, indicating that there exist strong geometry effects at a small aspect ratio. For large aspect ratio, the stability curve is less affected by the heat strength, and the critical Rayleigh number gradually approaches the critical value for a system with infinite horizontal extent [32]. The comparison of computed critical values at $\Gamma = 8$ with two-dimensional results [27] (Ra_{cr}^{2D}) and theoretical predictions [32] ($\mathrm{Ra}_{cr}^{\infty}$) is given in Table I. It can be seen that the critical Rayleigh numbers in the less confined cylinder are very close to the theoretical ones. It is worth noting that the instability for the onset of convection is supercritical in the confined cylinder rather than subcritical in a large or infinite horizontally extended system.

B. Secondary instability

When the primary instability is characterized by the axisymmetric mode, it is interesting to study the secondary instability. Depending on the control parameters, Ra, Pr, q, and Γ, the steady axisymmetric convective flow may undergo either oscillatory or steady bifurcation to become

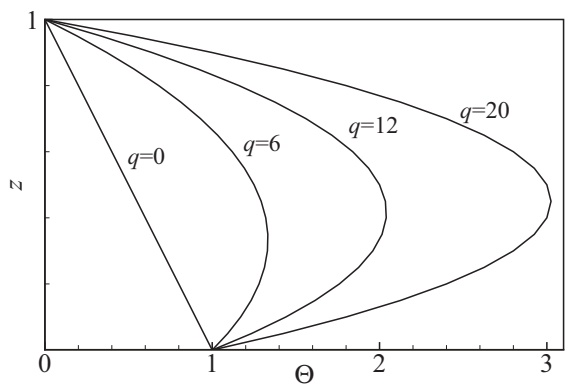

FIG. 1. Conductive temperature distribution for different heat strength.

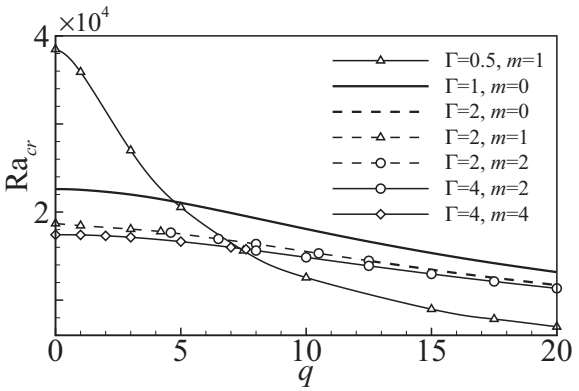

FIG. 2. Variation of critical Rayleigh number for onset of convection with heat strength at different aspect ratios.

three-dimensional flow or oscillatory axisymmetric flow as will be shown latter. The secondary instabilities for Rayleigh-Bénard convection in a cylinder have been studied extensively [33–37]. From the prior results on boundary-driven convection are expected to aid in understanding the secondary instability features of such dually driven flows. The typical aspect ratio $\Gamma = 1$ is chosen for secondary instability analysis. We first studied the effect of heat strength on the instability under three fixed Prandtl nubmers, i.e., $\mathrm{Pr} = 0.02$, $\mathrm{Pr} = 0.4$, and $\mathrm{Pr} = 1$, respectively. Then the influence of Prandtl number is studied at a moderate internal heat strength number $q = 6.4$.

The axisymmetric base flows for $\mathrm{Pr} = 0.02$, $\mathrm{Pr} = 0.4$, and $\mathrm{Pr} = 1$ are shown in Figs. 3, 4, and 5, respectively. For each Prandtl number, three internal heat strength numbers are chosen, $q = 3$, $q = 8$ and $q = 16$, to represent base flow structures under weak, moderate, and strong internal heat situation. In all cases, base flows are plotted on the meridional planes $(r,z) \in [-1,1] \times [0,1]$ with streamlines drawn in the left frames and isothermals drawn in the right frames. The axisymmetric convective flow has two forms: one is the hot fluid that rises along the sidewall and descends along the axis, and the other is hot fluid that ascends along the axis and descends along the sidewall, which are similar to axisymmetric base flows for Rayleigh-Bénard convection. These two forms have the same stability properties.

For $\mathrm{Pr} = 0.02$, as shown in Fig. 3, the base flows are drawn at $\mathrm{Ra} = 4000$, and a clockwise toroidal roll structure is exhibited by contours of stream function. The flow strength increases as q increases. Most of the isothermals are almost uniformly distributed in the radial direction due to strong thermal diffusivity of a small Prandtl number fluid. The largest temperature increases with increasing q, and the

TABLE I. Comparison of critical Rayleigh number at $\Gamma = 8$ with theoretical values [32] $\mathrm{Ra}_{cr}^{\infty}$ and two dimensional results [27] Ra_{cr}^{2D} (the ratio of width to height is 5π).

q	0	1	2	3	5	6	8	10	20
$\mathrm{Ra}_{cr}^{\infty}$	1708	1704	1695	1679	1633	-	-	1463	-
Ra_{cr}^{2D}	1739	1737	1727	1711	1663	1632	1562	1487	1130
Present	1716	1713	1703	1688	1641	1611	1543	1468	1121

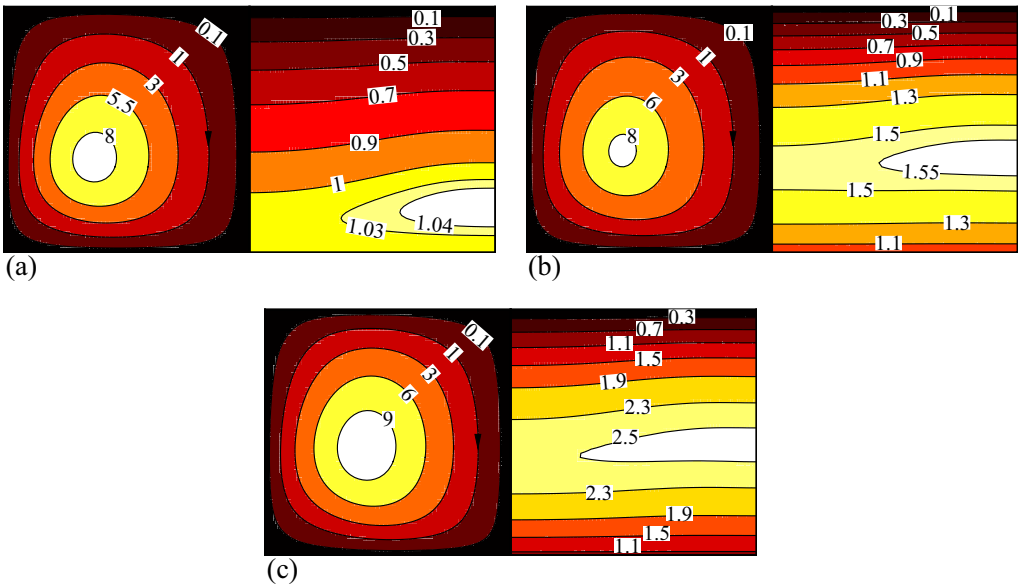

FIG. 3. Axisymmetric base flow at Pr = 0.02, Ra = 4000, and $q = 3$ (a), $q = 8$ (b), $q = 16$ (c). Left: Stream function contours. Right: Isotherms.

vertical position of the largest value increases as well. The enhancement of Rayleigh-Bénard instability by internal heat can be expected from the temperature distribution. It should be noted here that a stably stratified layer forms near the bottom. This kind of base flow structure is comparable with that of thermal convection in a laterally heated cylinder [38], where an unstably stratified layer is located above a stably stratified layer. Such stratification greatly affects the flow instability. Similar to the Pr = 0.02 case, the base flow for Pr = 0.4 is also characterized by a single toroidal roll structure, whereas counterclockwise rolls are plotted in Fig. 4. The difference is the location of maximum stream function located at a higher position manifesting the increase of buoyancy effect. Furthermore, the isothermals are curved in the middle of the cylinder related to the lower thermal diffusivity of fluid with a higher Prandtl number, and the radial temperature gradient is clearly exhibited. For Pr = 1, the axisymmetric base flows consist of two toroidal rolls. The flow structure displayed in Fig. 5(a) for $q = 3$ shows an unstable distribution where a larger convection roll is located above a smaller roll. The two convection rolls lying alongside are obtained at higher internal heat strength numbers as shown in Figs. 5(b) and 5(c). The isothermals in this case are significantly distorted, especially for large values of q. There are a large vertical and horizontal temperature gradient in the upper half of the cylinder.

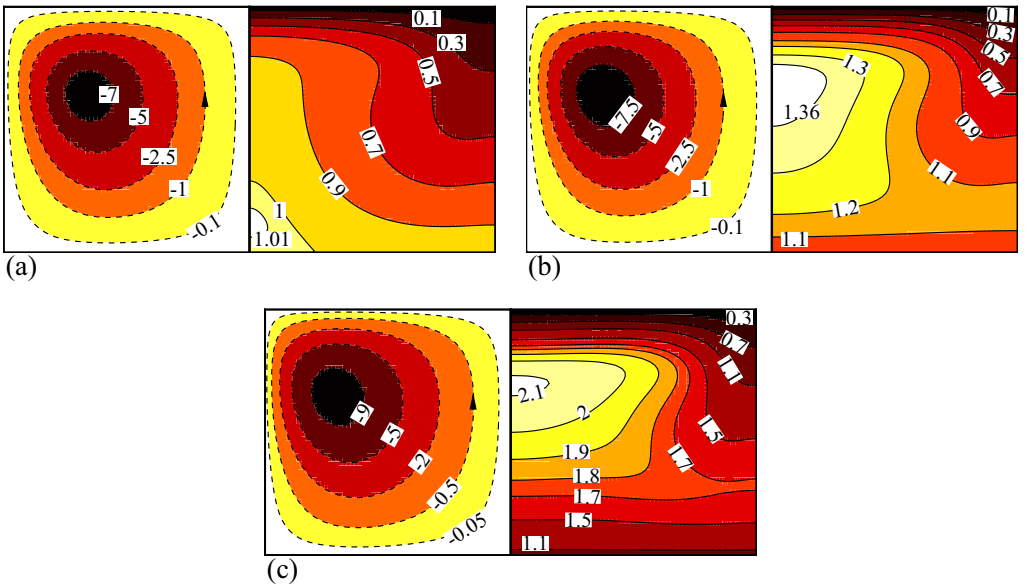

FIG. 4. Axisymmetric base flow at Pr = 0.4, Ra = 10 000, and $q = 3$ (a), $q = 8$ (b), $q = 16$ (c). Left: Stream function contours. Right: Isotherms.

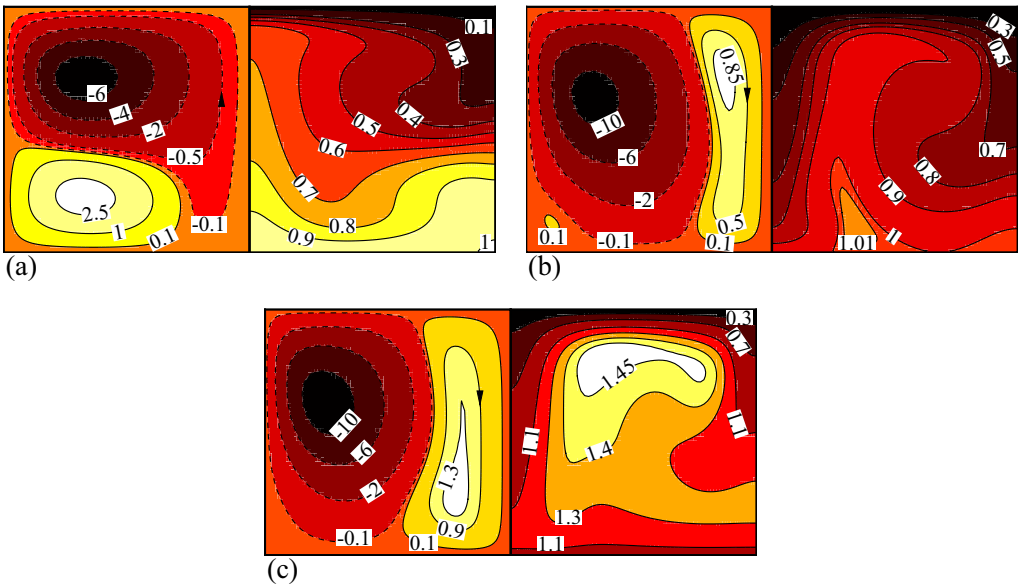

FIG. 5. Axisymmetric base flow at Pr = 1, Ra = 80 000, and $q = 3$ (a), $q = 8$ (b), $q = 16$ (c). Left: Stream function contours. Right: Isotherms.

Stability curves displaying the dependence of the critical Rayleigh number on the internal heat strength for three fixed values of the Prandtl number are shown in Figs. 6(a)–6(c). As shown in Fig. 6(a), the critical mode for the axisymmetry-breaking instability at Pr = 0.02 is steady, $m = 2$, for the studied heat strength range $0 < q < 20$. The internal heating has little effect on the stability of axisymmetric flow when the heat strength $q < 2$, where the critical Rayleigh number does not change much. When the heat strength is in the range $2 < q < 6$, the stability curve is multivalued. There are three critical Rayleigh numbers for a fixed q. The critical Rayleigh number decreases with increasing q as $6 < q < 20$, corresponding to the destabilize effect of strong internal heating. The multivalued stability curve is usually caused by

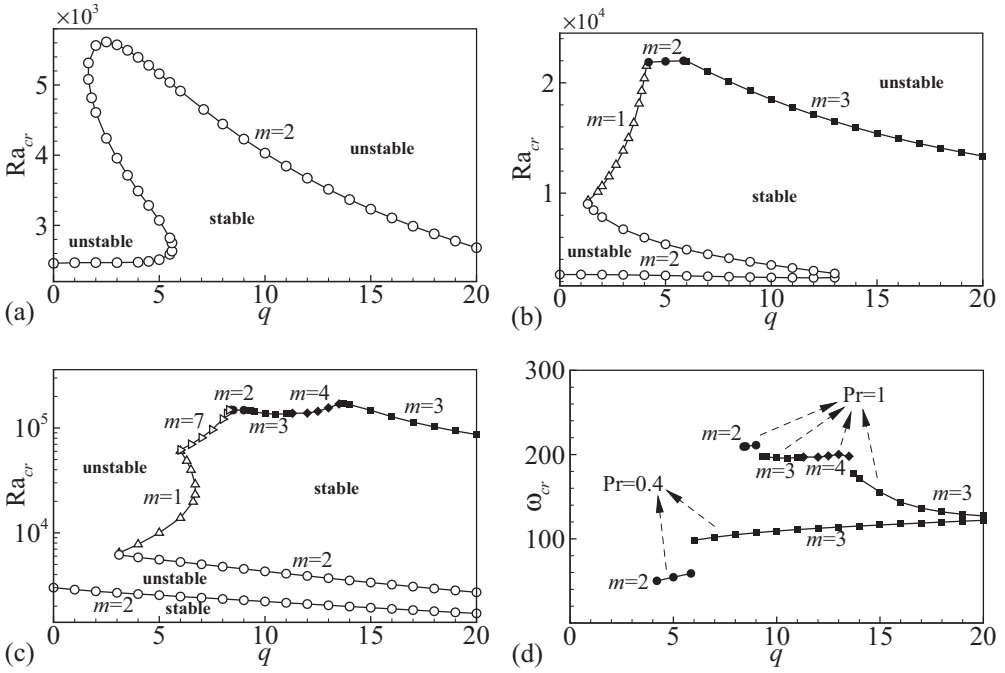

FIG. 6. Critical Rayleigh number, Ra_{cr}, as a function of the internal heat strength, q, for the transition from the basic state to different three-dimensional states for Pr = 0.02 (a), Pr = 0.4 (b), and Pr = 1 (c). Note that the vertical coordinate for panel (c) is plotted in natural logarithm scale. In panel (d) the critical circular frequency, ω_{cr}, as a function of the internal heat strength, q, for the unsteady transitions occurred in panels (b) and (c) are plotted. Solid curves with hollow symbols represent steady transitions and filled symbols oscillatory transitions.

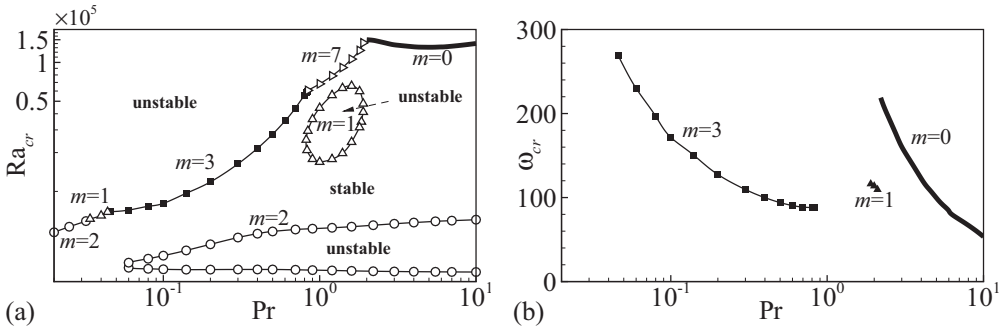

FIG. 7. (a) Ra_{cr} as a function of Pr for $q = 6.4$. (b) Critical circular frequency ω_{cr} as a function of Pr for $q = 6.4$. The horizontal coordinates and vertical coordinate in panel (a) are plotted in natural logarithm scale. Solid curves with hollow symbols represent steady transitions and filled symbols oscillatory transitions.

competition of several instability mechanisms; here it refers to buoyancy instability and hydrodynamic instability. Similar stability curves have been found in Rayleigh-Bénard convection [34,37] and laterally heated convection in cylinders at larger Prandtl numbers [38], whereas hydrodynamic instability is dominant for low Prandtl number convection in these two configurations. The convection with an internal heat source considered in this study actually enhances the buoyancy effect, which interacts with hydrodynamic instability thus bringing about the multivalued stability curve even at a low Prandtl number.

The stability curve for $\mathrm{Pr} = 0.4$ is illustrated in Fig. 6(b). Two steady instability modes $m = 1$ and $m = 2$ as well as two oscillatory instability modes $m = 2$ and $m = 3$ are obtained. These instability modes often appear in convection in a cylinder without internal heating. The range of q for multivalued critical Rayleigh number becomes much larger, from around 1.5 to 13. The critical Rayleigh number at the lower branch of the folded curve is small and varies little with q, while the critical value at the upper branch is large. For $\mathrm{Pr} = 1$ shown in Fig. 6(c), the stability curve becomes more complicated. Three steady instability modes $m = 1$, $m = 2$, $m = 7$ and three oscillatory instability modes $m = 2$, $m = 3$, $m = 4$ are obtained. The hysteresis range for q is further extended. The value of q is up to 20 in this study. Multiple critical Rayleigh numbers surely exist at higher q. The critical Rayleigh number at the lower branch of the curve decreases with increasing q. The critical value at the upper branch is one order larger. There exist five critical Rayleigh numbers in a narrow range of q around $q = 6$. Intense interaction of buoyancy instability and hydrodynamic instability arises for large-Prandtl-number flow as revealed from Figs. 6(b) and 6(c), especially at moderate to high internal heating numbers, resulting in the complex stability curves. The critical circular frequencies corresponding to the oscillatory critical modes for $\mathrm{Pr} = 0.4$ and $\mathrm{Pr} = 1$ are shown in Fig. 6(d). The critical frequency for convection with internal heat generation is much higher than that for pure Rayleigh-Bénard convection in a cylinder [37].

When q is of a moderate value, such as the value of q around 6, the interactions of different instability mechanisms are very strong as reflected in the multivalued stability curves in Fig. 6. Therefore we are motivated to study the secondary instability at a moderate internal heating number ($q = 6.4$). The variation of critical Rayleigh number with Prandlt number at $q = 6.4$ is shown in Fig. 7(a). The studied Prandtl number range is from 0.02 to 10. There is only one critical Rayleigh number for $\mathrm{Pr} < 0.06$. The stability curve becomes multivalued for $0.06 < \mathrm{Pr} < 10$. We calculated the critical Rayleigh number for large Prandtl number $\mathrm{Pr} = 100$, and three critical values can still be obtained. Similar to results in Fig. 6, the steady $m = 2$ mode is encountered at low Rayleigh number. The axisymmetric flow loses stability at a Rayleigh number around 2400 and becomes stable again at a little higher Rayleigh number. With the further increase of Rayleigh number, the critical Rayleigh number for the axisymmetric breaking instability is very large. The base flow loses stability to three-dimensional periodic flow with azimuthal wave number $m = 3$ in $0.05 < \mathrm{Pr} < 0.83$, steady flow with $m = 7$ in $0.83 < \mathrm{Pr} < 1.9$, periodic flow with $m = 1$ in $1.9 < \mathrm{Pr} < 2.1$, and periodic axisymmetric flow for $\mathrm{Pr} > 2.1$. The periodic $m = 1$ mode is not shown clearly in the figure as this range is too narrow. Note that the

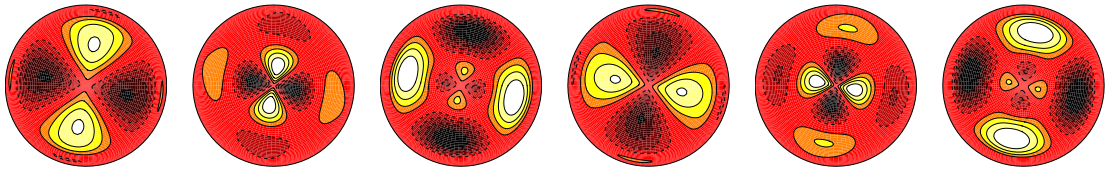

FIG. 8. Contours of azimuthal velocity on the $z = 0.8$ plane in a period at $q = 9$, $\mathrm{Pr} = 1$, $\mathrm{Ra} = 1.52 \times 10^5$, oscillation period $T = 0.0294$, and patterns at $t = 0, T/6, 2T/6, 3T/6, 4T/6$, and $5T/6$ are plotted. Eight levels are drawn between the values of -2 and 2. Light area (solid lines) represents positive value, and dark area (dashed lines) represents negative value.

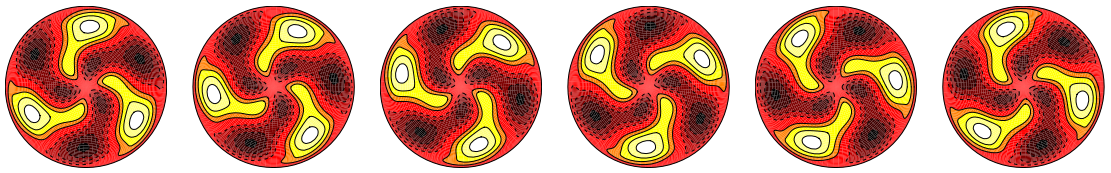

FIG. 9. Contours of azimuthal velocity on the $z = 0.8$ plane in a period at $q = 10$, $\mathrm{Pr} = 1$, $\mathrm{Ra} = 1.4 \times 10^5$, oscillation period $T = 0.0317$, and patterns at $t = 0, T/6, 2T/6, 3T/6, 4T/6$, and $5T/6$ are plotted. Eight levels are drawn between the values of -2 and 2. Light area (solid lines) represents positive value, and dark area (dashed lines) represents negative value.

oscillatory axisymmetric mode is predominant in a large range of Prandtl number, so far as we have calculated up to $\mathrm{Pr} = 100$. Moreover there is a closed curve which encloses an unstable region characterized by the $m = 1$ mode. The instability island is also observed in convection in a laterally heated cylinder [38]. The closed curve appears at Pr around 1, where thermal diffusivity and momentum diffusivity are comparable, thus the competition between buoyancy instability and hydrodynamic instability again results in this stability curve. The variation of critical circular frequency with Prandtl number is shown in Fig. 7(b). For each oscillatory mode, the critical circular frequency decreases with increasing Pr.

C. Three-dimensional oscillatory flow

The transition from an axisymmetric stationary flow to three-dimensional stationary or time-dependent flows can be predicted by linear stability analysis. However, nonlinear simulations are still required to determine flow structures and their evolutions. Some typical three-dimensional oscillatory flows are given below.

As seen from Fig. 6(c), bifurcations from a nontrivial base flow to periodic flows with azimuthal wave numbers $m = 2$, $m = 3$, and $m = 4$ are observed. The corresponding flow patterns shown by azimuthal velocity on the $z = 0.8$ plane over a period are given in Figs. 8, 9, and 10, respectively. The flow triggered by $m = 2$ oscillatory instability exhibits a standing wave state (Fig. 8). The periodic flows induced by $m = 3$ and $m = 4$ instabilities are obviously traveling waves, as illustrated in Figs. 9 and 10. The Rayleigh numbers for nonlinear simulations are quite near the critical value, thus the nonlinear frequencies are in agreement with the predicted values in Fig. 6(d). These oscillatory patterns are very similar to that found in Rayleigh-Bénard convection in a cylinder [36,37]

In Fig. 7(a), an axisymmetric oscillatory instability is obtained for $q = 6.4$, $\Gamma = 1$, and $\mathrm{Pr} > 2.1$, which has not been reported in thermal convection in a cylinder before. Taking $\mathrm{Pr} = 6.7$ as an example, the critical Rayleigh number for the $m = 0$ oscillatory instability is 1.329×10^5. The axisymmetric unsteady flow will lose stability to three-dimensional oscillatory state with increasing Ra, and the corresponding critical Ra determined by nonlinear simulation is 1.433×10^5. The nonaxisymmetric unsteady flow obtained at $\mathrm{Ra} = 1.45 \times 10^5$ is shown in Fig. 11. The flow is reflection symmetric about a meridional plane at each instant.

IV. CONCLUSION

The flow instabilities of thermal convection in a cylinder driven by both boundary heating and internal heating have been studied. The stability for the onset of convection and for axisymmetric steady state have been considered. The convection thresholds have been determined under different internal heat strength and aspect ratio. The critical Rayleigh number approaches the theoretical predictions for convection between infinite plates. The stability of axisymmetric steady base flow is studied for a fixed aspect ratio $\Gamma = 1$ and three Prandtl numbers $\mathrm{Pr} = 0.02$, $\mathrm{Pr} = 0.4$, and $\mathrm{Pr} = 1$. Strong dependence on both the Prandtl number and internal heat strength have been revealed. With regard to the strength of internal heat source, the flow instability is less affected at small q, and its properties are similar to convection without an internal heat source. When q increases to moderate values, the enhanced unstably stratified upper layer significantly modifies the flow instability. The strong interaction of buoyancy instability and hydrodynamic instability leads to more complicate instability phenomena than sole boundary driven convection. The curve is multivalued even at a low Prandtl number. At a higher Prandtl number ($\mathrm{Pr} = 1$), five critical Rayleigh numbers can be observed in the moderate internal heat strength range. When q is large enough, the stability curve becomes single valued for $\mathrm{Pr} = 0.02$ and $\mathrm{Pr} = 0.4$, except for $\mathrm{Pr} = 1$. A particular moderate internal heat strength $q = 6.4$ is chosen

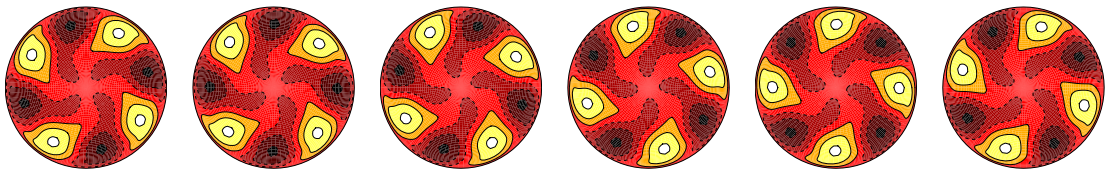

FIG. 10. Contours of azimuthal velocity on the $z = 0.8$ plane in a period at $q = 12$, $\mathrm{Pr} = 1$, $\mathrm{Ra} = 1.42 \times 10^5$, oscillation period $T = 0.0315$, and patterns at $t = 0, T/6, 2T/6, 3T/6, 4T/6$, and $5T/6$ are plotted. Six levels are drawn between the values of -1.4 and 1.5. Light area (solid lines) represents positive value, and dark area (dashed lines) represents negative value.

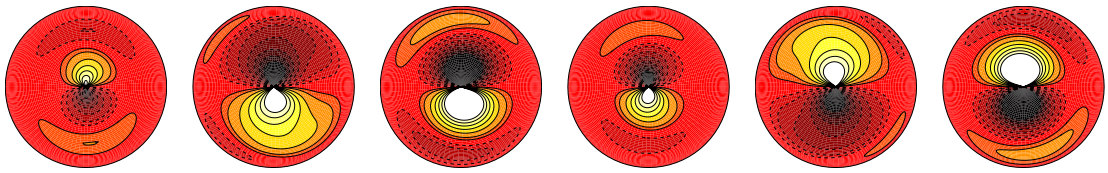

FIG. 11. Contours of azimuthal velocity on the $z = 0.8$ plane in a period at $q = 6.4$, $\mathrm{Pr} = 6.7$, $\mathrm{Ra} = 1.45 \times 10^5$, oscillation period $T = 0.161$, and patterns at $t = 0, T/6, 2T/6, 3T/6, 4T/6$, and $5T/6$ are plotted. Eight levels are drawn between the values of -1.2 and 1.2. Light area (solid lines) represents positive value, and dark area (dashed lines) represents negative value.

to study the influence of Prandtl number. The stability curve is also found to be multivalued as $\mathrm{Pr} > 0.06$. A new unsteady instability mode with azimuthal wave number zero has been observed. Finally, nonlinear simulations are conducted to study the flow patterns. The $m = 0$ periodic flow loses stability to three-dimensional unsteady flow through a supercritical Hopf bifurcation.

ACKNOWLEDGMENTS

This research is supported by the National Natural Science Foundation of China (NSFC) under Grants Nos. 11502137, 11402262, 11572314, and 11232011, and Z.W. especially thanks the Fundamental Research Funds for the Central Universities for their support.

[1] D. L. Turcotte and G. Schubert (eds.), *Geodynamics* (Cambridge University Press, Cambridge, 2001).
[2] K. A. Emanuel (ed.), *Atmospheric Convection* (Oxford University Press New York, 1994).
[3] E. Bodenschatz, W. Pesch, and G. Ahlers, Annu. Rev. Fluid Mech. **32**, 709 (2000).
[4] P. M. Patil and P. S. Kulkarni, Int. J. Therm. Sci. **47**, 1043 (2008).
[5] D. Goluskin, *Internally Heated Convection and Rayleigh-Bénard Convection* (Springer International Publishing, Switzerland, 2016).
[6] D. J. Tritton and M. N. Zarraga, J. Fluid Mech. **30**, 21 (1967).
[7] P. H. Roberts, J. Fluid Mech. **30**, 33 (1967).
[8] R. Thirby, J. Fluid Mech. **44**, 673 (1970).
[9] M. Tveitereid and E. Palm, J. Fluid Mech. **76**, 481 (1976).
[10] Y. Tasaka, Y. Kudoh, Y. Takeda, and T. Yanagisawa, J. Phys.: Conf. Ser. **14**, 168 (2005).
[11] Y. Tasaka, K. Yonekura, Y. Takeda, and T. Yanagisawa, J. Visualization **11**, 213 (2008).
[12] H. Ichikawa, K. Kurita, Y. Yamagishi, and T. Yanagisawa, Phys. Fluids **18**, 038101 (2006).
[13] F. A. Kulacki and R. J. Goldstein, J. Fluid Mech. **55**, 271 (1972).
[14] M. Jahn and H. H. Reineke, Proc. 5th Int. Heat Transfer Conf. **13** (1974).
[15] M. Tveitereid, Int. J. Heat Mass Transf. **21**, 335 (1978).
[16] S. D. Lee, J. K. Lee, and K. Y. Suh, J. Heat Transfer **129**, 679 (2007).
[17] R. S. Peckover and I. H. Hutchinson, Phys. Fluids **17**, 1369 (1974).
[18] M. Wörner, M. Schmidt, and G. Grötzbach, J. Hydraul. Res. **35**, 773 (1997).
[19] J. P. Whitehead and C. R. Doering, J. Math. Phys. **52**, 093101 (2011).
[20] P. Deshmukh, S. K. Mitra, and U. N. Gaitonde, Int. J. Heat Mass Transf. **54**, 1465 (2011).
[21] D. Goluskin and E. A. Spiegel, Phys. Lett. A **377**, 83 (2012).
[22] D. Goluskin and E. A. Spiegel, J. Fluid Mech. **791**, R6 (2016).
[23] R. Nourgaliev, T. Dinh, and B. Sehgal, Nucl. Eng. Des. **169**, 165 (1997).
[24] G. Grötzbach and M. Wörner, Int. J. Heat Fluid Flow **20**, 222 (1999).
[25] S. D. Lee, J. K. Lee, and K. Y. Suh, Nucl. Eng. Des. **237**, 473 (2007).
[26] G. K. Perekattu and C. Balaji, Int. J. Heat Mass Transfer **52**, 4254 (2009).
[27] V. V. Kolmychkov, O. S. Mazhorova, and O. V. Shcheritsa, Phys. Lett. A **377**, 2111 (2013).
[28] R. Verzicco and P. Orlandi, J. Comput. Phys. **123**, 402 (1996).
[29] S. Hugues and A. Randriamampianina, Int. J. Num. Methods Fluids **28**, 501 (1998).
[30] L. S. Tuckerman and D. Barkley, in *Numerical Methods for Bifurcation Problems and Large-Scale Dynamical Systems*, Vol. 119, edited by E. Doedel and L. S. Tuckerman (Springer, New York, 2000), pp. 453–466.
[31] R. B. Lehoucq, D. C. Sorensen, and C. Yang (eds.), *ARPACK Users Guide:Solution of Large-Scale Eigenvalue Problems with Implicitly Restarted Arnoldi Methods* (SIAM, Philadelphia, 1998).
[32] E. M. Sparrow, R. J. Goldstein, and V. H. Johnsson, J. Fluid Mech. **18**, 513 (1964).
[33] G. Neumann, J. Fluid Mech. **214**, 559 (1990).
[34] M. Wanschura, H. C. Kuhlmann, and H. J. Rath, J. Fluid Mech. **326**, 399 (1996).
[35] R. Touihri, H. B. Hadid, and D. Henry, Phys. Fluids **11**, 2078 (1999).
[36] K. Borońska and L. S. Tuckerman, J. Fluid Mech. **559**, 279 (2006).
[37] B. F. Wang, D. J. Ma, C. Chen, and D. J. Sun, J. Fluid Mech. **711**, 27 (2012).
[38] B. F. Wang, Z. H. Wan, Z. W. Guo, D. J. Ma, and D. J. Sun, J. Fluid Mech. **747**, 447 (2014).